

Cyanide-Bridged Os(II)/Ln(III) Coordination Networks Containing [Os(phen)(CN)₄]²⁻ as an Energy Donor: Structural and Photophysical PropertiesSvetlana G. Baca,[†] Simon J. A. Pope,[‡] Harry Adams,[†] and Michael D. Ward^{*†}*Department of Chemistry, University of Sheffield, Sheffield S3 7HF, U.K., and School of Chemistry, Main Building, Cardiff University, Cardiff CF10 3AT, U.K.*

Received December 3, 2007

Slow evaporation of aqueous solutions containing mixtures of Na₂[Os(phen)(CN)₄], Ln(III) salts (Ln = Pr, Nd, Gd, Er, Yb), and (in some cases) an additional ligand such as 1,10-phenanthroline (phen) or 2,2'-bipyrimidine (bpym) afforded crystalline coordination networks in which the [Os(phen)(CN)₄]²⁻ anions are coordinated to Ln(III) cations via Os–CN–Ln cyanide bridges. The additional diimine ligands, if present, also coordinate to the Ln(III) centers. Several types of structure have been identified by X-ray crystallographic studies. Photophysical studies showed that the characteristic emission of the [Os(phen)(CN)₄]²⁻ chromophore, which occurs at ~680 nm in this type of coordination environment with a triplet metal-to-ligand charge transfer (³MLCT) energy content of ~16 000 cm⁻¹, is quenched by energy transfer to those Ln(III) centers (Pr, Nd, Er, Yb) that have low-lying f–f states capable of accepting energy from the Os(II)-based ³MLCT state. Time-resolved studies on the residual (partially quenched) Os(II)-based luminescence allowed the rates of Os(II) → Ln(III) energy transfer to be evaluated. The measured rates varied substantially, having values of >5 × 10⁸, ~1 × 10⁸, and 2.5 × 10⁷ s⁻¹ for Ln = Nd, Er or Yb, and Pr, respectively. These differing rates of Os(II) → Ln(III) energy transfer can be rationalized on the basis of the availability of f–f states of the different Ln(III) centers that are capable of acting as energy acceptors. In general, the rates of Os(II) → Ln(III) energy transfer are an order of magnitude faster than the rates of Ru(II) → Ln(III) energy transfer in a previously described series of [Ru(bpym)(CN)₄]²⁻/Ln(III) networks. This is ascribed principally to the lower energy of the Os(II)-based ³MLCT state, which provides better spectroscopic overlap with the low-lying f–f states of the Ln(III) ions.

Introduction

In a series of recent papers we have described studies of the structural and photophysical properties of coordination networks in which luminescent cyanometallate anions are combined with lanthanide cations such as Yb(III), Nd(III), Er(III), and Pr(III), which can display near-infrared luminescence from low-energy f–f states.^{1–3} Lanthanide/cyanometallate networks have been studied by many groups,^{4–6} largely in regard to a combination of their structural⁴ and magnetic⁵ properties, although there has also been some interest in their photophysical properties.⁶

From a structural point of view, these materials are of interest because they display a range of unusual structural types based on attachment of the cyanide N-donors of the d-block cyanometallate units to the Ln(III) centers, affording networks based on M¹–CN–M² linkages (where M¹ is the d-block metal and M² is the lanthanide ion). Cyanometallate anions such as {[Ru(CN)₄]₂(μ-bpym)}⁴⁻ (bpym = 2,2'-bipyrimidine) and {[Ru(CN)₄]₃(μ-HAT)}⁶⁻ (HAT = hexaaza-triphenylene), which contain eight and twelve externally directed cyanide groups, respectively, can act as “tectons”

* To whom correspondence should be addressed. E-mail: m.d.ward@sheffield.ac.uk.

[†] University of Sheffield.

[‡] Cardiff University.

(1) (a) Davies, G. M.; Pope, S. J. A.; Adams, H.; Faulkner, S.; Ward, M. D. *Inorg. Chem.* **2005**, *44*, 4656. (b) Herrera, J.-M.; Pope, S. J. A.; Adams, H.; Faulkner, S.; Ward, M. D. *Inorg. Chem.* **2006**, *45*, 3895. (c) Adams, H.; Alsindi, W. Z.; Davies, G. M.; Duriska, M. B.; Easun, T. L.; Fenton, H. E.; Herrera, J.-M.; George, M. W.; Ronayne, K. L.; Sun, X.-Z.; Towrie, M.; Ward, M. D. *Dalton Trans.* **2006**, 39. (d) Baca, S. G.; Adams, H.; Sykes, D.; Faulkner, S.; Ward, M. D. *Dalton Trans.* **2007**, 2419.

having greater potential connectivities at a single cyanometallate fragment than can be provided by mononuclear cyanometallates alone.² From a photophysical point of view, these materials have allowed us to study how absorption of light in the visible region by a d-block component such as [Ru(bipy)(CN)₄]²⁻, with a long-lived triplet metal-to-ligand charge transfer (³MLCT) excited state, is followed by sensitized near-infrared luminescence from the Ln(III) component as a consequence of d → f energy transfer. Different combinations of d- and f-block components have shown that energy transfer rates across the M¹–CN–M² linkage can vary over 2 orders of magnitude according to the spectroscopic overlap between the emission spectrum of the donor unit and the f–f absorption spectrum of the acceptor unit.¹ In one case, using [Cr(CN)₆]³⁻ as the d-block component, we were able to unambiguously prove that the d → f energy transfer occurred via the Dexter mechanism.³

In this paper we report on a series of compounds containing the d-block unit [Os(phen)(CN)₄]²⁻ in combination with various near-IR-emissive Ln(III) cations. From a structural point of view, the resulting networks were not expected to differ substantially from those afforded by combination of [Ru(phen)(CN)₄]²⁻ (phen = 1,10-phenanthroline) or [Ru(bipy)(CN)₄]²⁻ (bipy = 2,2'-bipyridine) with Ln(III) cations.¹ From a photophysical perspective, however, the materials were expected to be quite different, because complexes of the [Os(diimine)(CN)₄]²⁻ type have lower-energy absorption and emission properties than their Ru(II) analogues^{7,8} (as illustrated by the difference between [Ru(bipy)₃]²⁺ and [Os(bipy)₃]²⁺). Complexes of the type [Os(diimine)(CN)₄]²⁻ have scarcely been studied,^{7,8} and there are no reports of their use as energy donors in supramolecular assemblies. There are two reasons why [Os(phen)(CN)₄]²⁻/Ln(III) networks should be of photophysical interest. First, the low energy of their MLCT absorptions should permit generation of sensitized near-IR luminescence from Ln(III) centers using relatively long wavelength excitation, an important goal that has prompted several groups to use chromophores that absorb at long wavelengths as sensitizers for near-IR Ln(III)-based luminescence.⁹ Second, the low energy of the ³MLCT emission should be a good match for the low-energy f–f excited states that generate near-IR luminescence from lanthanide(III) ions, so Os → Ln energy transfer could be more efficient than Ru → Ln energy transfer in some cases.

Results and Discussion

Syntheses and Structural Properties. All of the crystalline materials were simply prepared by the same general method, namely, slow evaporation of water/acetone or water/methanol solutions containing an equimolar mixture of Na₂[Os(phen)(CN)₄], the appropriate Ln(III) nitrate salt, and (in some cases) an ancillary polypyridine-type ligand (bpym or phen). The addition of phen or bpym to the mixtures results in coordination of these ligands to the Ln(III) centers in the resultant networks, occupying sites that would otherwise contain solvent or cyanide ligands, thereby altering the structures and the degrees of cyanide-based cross-linking in the networks. The materials were characterized by single-crystal X-ray diffraction studies, using elemental analysis and IR spectra to confirm the homogeneity of bulk samples. Five different structural types of material have been identified, and a representative example of each type is discussed here. Selected bond distances around the Ln(III) center for the five structures discussed in detail are collected in Table 1. In every case, the [Os(phen)(CN)₄]²⁻ units are structurally

- (2) (a) Herrera, J.-M.; Ward, M. D.; Adams, H.; Pope, S. J. A.; Faulkner, S. *Chem. Commun.* **2006**, 1851. (b) Herrera, J.-M.; Pope, S. J. A.; Meijer, A. J. H. M.; Easun, T. L.; Adams, H.; Alsimdi, W. Z.; Sun, X.-Z.; George, M. W.; Faulkner, S.; Ward, M. D. *J. Am. Chem. Soc.* **2007**, *129*, 11491.
- (3) Lazarides, T.; Davies, G. M.; Adams, H.; Sabatini, C.; Barigelletti, F.; Barbieri, A.; Pope, S. J. A.; Faulkner, S.; Ward, M. D. *Photochem. Photobiol. Sci.* **2007**, *6*, 1152.
- (4) (a) Liu, S.; Meyers, E. A.; Shore, S. G. *Angew. Chem., Int. Ed.* **2002**, *41*, 3609. (b) Plecnik, C. E.; Liu, S.; Shore, S. G. *Acc. Chem. Res.* **2003**, *36*, 499. and references therein. (c) Goubard, F.; Tabuteau, A. *Struct. Chem.* **2003**, *14*, 257. (d) Mullica, D. F.; Farmer, J. M.; Cunningham, B. P.; Kautz, J. A. *J. Coord. Chem.* **2000**, *49*, 239. (e) Kautz, J. A.; Mullica, D. F.; Cunningham, B. P.; Coombs, R. A.; Farmer, J. M. *J. Mol. Struct.* **2000**, *523*, 175. (f) Mullica, D. F.; Farmer, J. M.; Kautz, J. A. *Inorg. Chem. Commun.* **1999**, *2*, 73. (g) Miller, T. A.; Jeffery, J. C.; Ward, M. D. *CrystEngComm* **2003**, *5*, 495.

- (5) (a) Ma, B.-Q.; Gao, S.; Su, G.; Xu, G.-X. *Angew. Chem., Int. Ed.* **2001**, *40*, 434. (b) Figuerola, A.; Diaz, C.; Ribas, J.; Tangoulis, V.; Granell, J.; Lloret, F.; Mahia, J.; Maestro, M. *Inorg. Chem.* **2003**, *42*, 641. (c) Toma, L. M.; Delgado, F. S.; Ruiz-Pérez, C.; Carrasco, R.; Cano, J.; Lloret, F.; Julve, M. *Dalton Trans.* **2004**, 2836. (d) Herrera, J.-M.; Marvaud, V.; Verdager, M.; Marrot, J.; Kalisz, M.; Mathonière, C. *Angew. Chem., Int. Ed.* **2004**, *43*, 5468. (e) Figuerola, A.; Diaz, C.; El Fallah, M. S.; Ribas, J.; Maestro, M.; Mahia, J. *Chem. Commun.* **2001**, 1204. (f) Figuerola, A.; Ribas, J.; Casanova, D.; Maestro, M.; Alvarez, S.; Diaz, C. *Inorg. Chem.* **2005**, *44*, 6949.
- (6) (a) Rawashdeh-Omary, M. A.; Larochele, C. L.; Patterson, H. H. *Inorg. Chem.* **2000**, *39*, 4527. (b) Assefa, Z.; Shankle, G.; Patterson, H. H.; Reynolds, R. *Inorg. Chem.* **1994**, *33*, 2187. (c) Guo, Z. H.; Yson, R. L.; Patterson, H. H. *Chem. Phys. Lett.* **2007**, *445*, 340. (d) Colis, J. C. F.; Larochele, C.; Staples, R.; Herbst-Irmer, R.; Patterson, H. H. *Dalton Trans.* **2005**, 675. (e) Colis, J. C. F.; Larochele, C.; Fernandez, E. J.; Lopez-De-Luzuriaga, J. M.; Monge, M.; Laguna, A.; Tripp, C.; Patterson, H. J. *Phys. Chem. B* **2005**, *109*, 4317. (f) Colis, J. C. F.; Staples, R.; Tripp, C.; Labrecque, D.; Patterson, H. J. *Phys. Chem. B* **2005**, *109*, 102. (g) Kunkely, H.; Vogler, A. *Inorg. Chem. Commun.* **2004**, *7*, 770.
- (7) Baca, S. G.; Adams, H.; Grange, C. S.; Smith, A. P.; Sazanovich, I.; Ward, M. D. *Inorg. Chem.* **2007**, *46*, 9779.
- (8) García Posse, M. E.; Katz, N. E.; Baraldo, L. M.; Polonuer, D. D.; Colombano, C. G.; Olabe, J. A. *Inorg. Chem.* **1995**, *34*, 1830.
- (9) (a) Klink, S. I.; Keizer, H.; van Veggel, F. C. J. M. *Angew. Chem., Int. Ed.* **2000**, *39*, 4319. (b) Beeby, A.; Dickins, R. S.; FitzGerald, S.; Govenlock, L. J.; Maupin, C. L.; Parker, D.; Riehl, J. P.; Siligardi, G.; Williams, J. A. G. *Chem. Commun.* **2000**, 1183. (c) Imbert, D.; Cantuel, M.; Bünzli, J.-C. G.; Bernardinelli, G.; Piguet, C. *J. Am. Chem. Soc.* **2003**, *125*, 15698. (d) Torelli, S.; Imbert, D.; Cantuel, M.; Bernardinelli, G.; Delahaye, S.; Hauser, A.; Bünzli, J.-C. G.; Piguet, C. *Chem.—Eur. J.* **2005**, *11*, 3228. (e) Pope, S. J. A.; Coe, B. J.; Faulkner, S. *Chem. Commun.* **2004**, 1550. (f) Pope, S. J. A.; Coe, B. J.; Faulkner, S.; Bichenkova, E. V.; Yu, X.; Douglas, K. T. *J. Am. Chem. Soc.* **2004**, *126*, 9490. (g) Guo, D.; Duan, C.-Y.; Lu, F.; Hasegawa, Y.; Meng, Q.-J.; Yanagida, S. *Chem. Commun.* **2004**, 1486. (h) Glover, P. B.; Ashton, P. R.; Childs, L. J.; Rodger, A.; Kercher, M.; Williams, R. M.; De Cola, L.; Pikramenou, Z. *J. Am. Chem. Soc.* **2003**, *125*, 9918. (i) Shavaleev, N. M.; Moorcraft, L. P.; Pope, S. J. A.; Bell, Z. R.; Faulkner, S.; Ward, M. D. *Chem. Commun.* **2003**, 1134. (j) Shavaleev, N. M.; Moorcraft, L. P.; Pope, S. J. A.; Bell, Z. R.; Faulkner, S.; Ward, M. D. *Chem.—Eur. J.* **2003**, *9*, 5283. (k) Shavaleev, N. M.; Accorsi, G.; Virgili, D.; Bell, Z. R.; Lazarides, T.; Calogero, G.; Armaroli, N.; Ward, M. D. *Inorg. Chem.* **2005**, *44*, 61. (l) Ronson, T. K.; Lazarides, T.; Adams, H.; Pope, S. J. A.; Sykes, D.; Faulkner, S.; Coles, S. J.; Hursthouse, M. B.; Clegg, W.; Harrington, R. W.; Ward, M. D. *Chem.—Eur. J.* **2006**, *12*, 9299. (m) Pope, S. J. A.; Burton-Pye, B. P.; Berridge, R.; Khan, T.; Skabara, P. J.; Faulkner, S. *J. Dalton Trans.* **2006**, 2907. (n) Ward, M. D. *Coord. Chem. Rev.* **2007**, *251*, 1663.

Table 1. Selected Bond Distances (Å) around the Ln(III) Centers in the Crystal Structures

bond	distance	bond	distance
Os–Gd^a			
Gd(1)–O(1)	2.377(2)	Gd(1)–O(2)	2.4325(19)
Gd(1)–O(4)	2.4011(19)	Gd(1)–N(3)	2.457(2)
Gd(1)–O(5)	2.4137(19)	Gd(1)–N(6B)	2.472(2)
Gd(1)–O(3)	2.4139(19)	Gd(1)–N(8)	2.483(2)
Os–Pr–PhenA^b			
Pr(1)–O(1)	2.451(6)	Pr(1)–N(16)	2.617(6)
Pr(1)–N(10A)	2.471(6)	Pr(1)–N(13)	2.629(6)
Pr(1)–N(9)	2.492(6)	Pr(1)–N(14)	2.666(6)
Pr(1)–N(3)	2.493(6)	Pr(1)–N(15)	2.674(5)
Os–Pr–PhenB^c			
Pr(1)–N(5A)	2.487(5)	Pr(2)–N(6C)	2.485(5)
Pr(1)–O(2)	2.495(4)	Pr(2)–O(3)	2.494(5)
Pr(1)–N(11B)	2.500(5)	Pr(2)–O(4)	2.502(4)
Pr(1)–O(1)	2.507(5)	Pr(2)–N(9)	2.504(6)
Pr(1)–N(4)	2.514(6)	Pr(2)–N(12D)	2.520(5)
Pr(1)–N(10)	2.530(6)	Pr(2)–O(3)	2.525(3)
Pr(1)–N(19)	2.675(5)	Pr(2)–N(21)	2.653(5)
Pr(1)–N(20)	2.693(5)	Pr(2)–N(22)	2.678(5)
Os–Er–BpymA			
Er(1)–O(4)	2.318(11)	Er(2)–O(3)	2.316(11)
Er(1)–O(6)	2.328(12)	Er(2)–O(1)	2.340(11)
Er(1)–N(4)	2.339(13)	Er(2)–N(10)	2.365(13)
Er(1)–O(5)	2.343(11)	Er(2)–N(15)	2.368(13)
Er(1)–N(9)	2.374(12)	Er(2)–O(2)	2.394(10)
Er(1)–O(7)	2.396(11)	Er(2)–N(3)	2.401(12)
Er(1)–N(19)	2.560(12)	Er(2)–N(22)	2.547(12)
Er(1)–N(20)	2.566(12)	Er(2)–N(21)	2.576(11)
Os–Nd–BpymB^d			
Nd(1)–N(3)	2.465(8)	Nd(3)–O(7)	2.483(7)
Nd(1)–O(2)	2.467(7)	Nd(3)–N(4A)	2.495(7)
Nd(1)–N(16)	2.479(8)	Nd(3)–N(15A)	2.498(8)
Nd(1)–O(1)	2.481(9)	Nd(3)–N(10)	2.527(8)
Nd(1)–N(21)	2.493(8)	Nd(3)–O(9)	2.542(7)
Nd(1)–N(33)	2.509(8)	Nd(3)–O(6)	2.543(6)
Nd(1)–N(37)	2.711(7)	Nd(3)–O(8)	2.546(7)
Nd(1)–N(40)	2.754(7)	Nd(3)–N(44)	2.694(8)
Nd(2)–O(3)	2.389(7)	Nd(3)–N(41)	2.780(8)
Nd(2)–N(9)	2.450(8)	Nd(4)–O(10)	2.425(8)
Nd(2)–N(27)	2.457(8)	Nd(4)–O(11)	2.432(7)
Nd(2)–N(34)	2.465(8)	Nd(4)–N(28B)	2.446(8)
Nd(2)–O(5)	2.465(8)	Nd(4)–O(13)	2.455(7)
Nd(2)–O(4)	2.494(7)	Nd(4)–N(22)	2.469(8)
Nd(2)–N(39)	2.690(8)	Nd(4)–O(12)	2.477(7)
Nd(2)–N(38)	2.691(7)	Nd(4)–N(43)	2.701(8)
		Nd(4)–N(42)	2.702(8)

^a Symmetry transformation to generate equivalent atoms A in **Os–Gd**: $x - 1/2, -y + 1/2, -z$. ^b Symmetry transformation to generate equivalent atoms B in **Os–Pr–PhenA**: $-x + 2, -y, -z + 2$. ^c Symmetry transformations to generate equivalent atoms in **Os–Pr–PhenB**: $x + 1, y, z$ for A; $-x + 1, -y + 1, -z + 1$ for B; $-x, -y + 1, -z + 1$ for C; $x - 1, y, z$ for D. ^d Symmetry transformations to generate equivalent atoms in **Os–Nd–BpymB**: $x + 1/2, -y + 1/2, z - 1/2$ for A; $x + 1, y, z$ for B.

similar and unremarkable, with Os–C distances in the range ~ 1.95 – 2.07 Å and slightly longer distances of ~ 2.10 – 2.16 Å between Os and the phen N atoms.

Crystals of $\{[\text{Os}(\text{phen})(\text{CN})_4]_{1.5}[\text{Gd}(\text{H}_2\text{O})_4(\text{MeOH})(\text{H}_2\text{O})_4]\}_\infty$ (**Os–Gd**) were grown by slow evaporation of a solution of $\text{Na}_2[\text{Os}(\text{phen})(\text{CN})_4]$ and $\text{Gd}(\text{NO}_3)_3 \cdot 6\text{H}_2\text{O}$ in aqueous methanol. The structure is shown in Figures 1 and 2 and consists of two-dimensional sheets, each of which has a sandwichlike structure. $[\text{Os}(\text{phen})(\text{CN})_4]^{2-}$ units at the “top” and “bottom” of each sheet (the layers of bread in the sandwich) have their cyanide groups directed toward the center of the sheet, where they interact

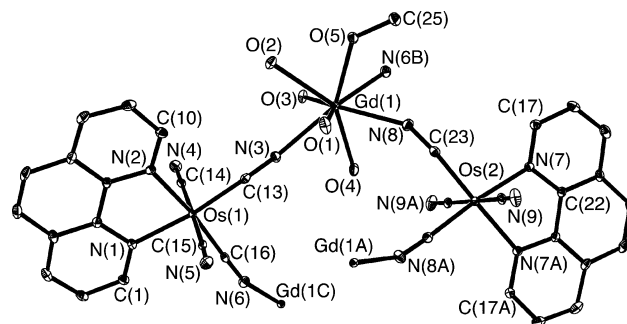


Figure 1. ORTEP view of the asymmetric unit of **Os–Gd**. H atoms and lattice solvent molecules have been omitted for clarity. A few extra atoms from adjacent asymmetric units have been added in order to complete the coordination spheres around the metal ions.

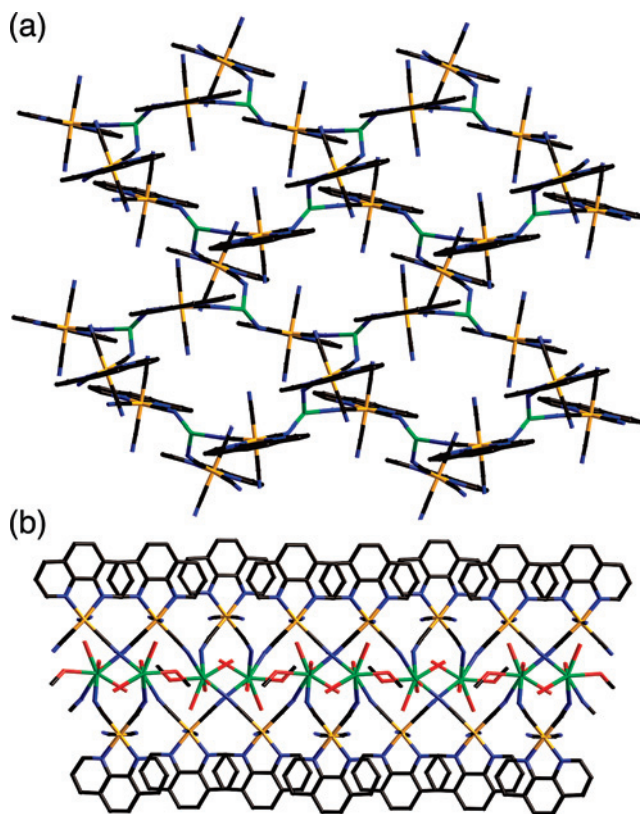


Figure 2. Two mutually perpendicular views of a layer in the structure of **Os–Gd**: (a) a top view looking directly down onto the layer (with water ligands omitted for clarity); (b) an edge-on view of the layer. (Color key: Gd, green; Os, orange; C, black; N, blue; O, red.)

with Gd(III) ions (the filling of the sandwich) by direct coordination and with water molecules by $\text{CN} \cdots \text{HOH}$ hydrogen bonds. In each $[\text{Os}(\text{phen})(\text{CN})_4]^{2-}$ unit, the two cyanides in the same plane as the phen ligand are coordinated to different Gd(III) centers, whereas the two axial (out-of-plane) cyanides are hydrogen-bonded to lattice water molecules with typical nonbonded $\text{N} \cdots \text{O}$ separations of 2.8 – 2.9 Å. Each Gd(III) center is eight-coordinate, having three cyanide donors (each from a different $[\text{Os}(\text{phen})(\text{CN})_4]^{2-}$ unit) along with four water molecules and one methanol molecule as additional ligands. Charge balance requires that there be 1.5 $[\text{Os}(\text{phen})(\text{CN})_4]^{2-}$ units per Gd(III) center; this results in three cyanide ligands being coordinated around each

Gd(III), since each $[\text{Os}(\text{phen})(\text{CN})_4]^{2-}$ unit uses two of its cyanides in Os–CN–Gd bridges. The Os···Gd separations vary, depending on the linearity of the bridging cyanide. Thus, the two independent Os(1)···Gd(1) distances are 5.59 and 5.47 Å, reflecting C–N–Gd angles of 175 and 153°, respectively; the Os(2)···Gd(1) distance of 5.29 Å is shorter, reflecting the more-bent cyanide coordination (having a C–N–Gd angle of 144°).

Slow evaporation of aqueous methanol solutions containing $\text{Na}_2[\text{Os}(\text{phen})(\text{CN})_4]$, the appropriate Ln(III) salt, and 2 equiv of additional phenanthroline afforded two types of crystal, depending on the conditions (see Table 2 for a summary of crystal and refinement data). The first type (obtained for Ln = Gd, Pr, Nd, Er, Yb) is exemplified by the structure $\text{Na}_2\{[\text{Os}(\text{phen})(\text{CN})_4]_4[\text{Pr}(\text{phen})_2(\text{H}_2\text{O})_2]_2\} \cdot 4\text{MeOH} \cdot 17\text{H}_2\text{O}$ (**Os–Pr–PhenA**), the most significant feature of which is the hexanuclear assembly containing three $[\text{Os}(\text{phen})(\text{CN})_4]^{2-}$ units and two $[\text{Pr}(\text{phen})_2(\text{H}_2\text{O})]^{3+}$ units, as shown in Figure 3. There is a central 12-membered $\text{Os}_2\text{Pr}_2(\mu\text{-CN})_4$ ring in which Os(II) and Pr(III) centers alternate at the corners and cyanide bridges form each of the four edges; in addition, two $[\text{Os}(\text{phen})(\text{CN})_4]^{2-}$ units [Os(1)/Os(1A)] are “pendent” from this central ring via single cyanide bridges to the Pr(III) ions. Each Pr(III) center is eight-coordinate, having two bidentate phen ligands, one water ligand, and three bridging cyanides, each from a different Os(II) center. Os(1) and Os(2) use one and two of their cyanides, respectively, as bridges to Pr(III); the additional phen ligands coordinated to the Pr(III) help to minimize the number of sites occupied by water ligands. Those cyanide groups that are not coordinated to Pr(III) centers are again involved in hydrogen bonding to lattice water molecules, with N···O separations of ~ 2.8 Å, but the extensive disorder of the lattice water molecules makes detailed analysis of this inappropriate. This type of hexanuclear assembly is generally similar to some we have observed previously in $[\text{Ru}(\text{phen})(\text{CN})_4]^{2-}/\text{Ln}(\text{III})$ salts.^{1d}

The second structural type was obtained by crystallizing $\text{Na}_2[\text{Os}(\text{phen})(\text{CN})_4]$ with a Ln(III) chloride salt (Ln = Pr, Nd) in the presence of added phenanthroline and is exemplified by $\{[\text{Os}(\text{phen})(\text{CN})_4]_3[\text{Pr}(\text{H}_2\text{O})_2(\text{phen})]_2(\text{H}_2\text{O})_{11.5}\}_\infty$ (**Os–Pr–PhenB**), whose structure is shown in Figures 4 and 5. The asymmetric unit of this compound contains three independent $[\text{Os}(\text{phen})(\text{CN})_4]^{2-}$ units and two independent $[\text{Pr}(\text{H}_2\text{O})_2(\text{phen})]^{3+}$ units (Figure 4). Of these, two of the three $[\text{Os}(\text{phen})(\text{CN})_4]^{2-}$ units [involving Os(1) and Os(2)] and the two $[\text{Pr}(\text{H}_2\text{O})_2(\text{phen})]^{3+}$ units are connected via cyanide bridges, forming a one-dimensional “tube” with an approximately square cross section. Each square consists of a 12-membered $\text{Os}_2\text{Pr}_2(\mu\text{-CN})_4$ ring; these are stacked vertically via additional cyanide bridges to give an infinite linear array of cyanide-bridged cubes in which metal types alternate at the corners (Figure 5), similar to a column extracted from a Prussian Blue-type structure. Each $[\text{Os}(\text{phen})(\text{CN})_4]^{2-}$ unit in this tubular assembly uses all four of its cyanide ligands to connect to different Pr(III) centers; the Pr(III) centers in turn are eight-coordinate, having four cyanide ligands, two water ligands, and the bidentate phenanthroline unit. The

Os···Pr distances across cyanide bridges vary from 5.32 to 5.70 Å, depending on the angle at the cyanide N atom: the longest Os···Pr separation corresponds to an almost perfectly linear C–N–Pr interaction (with a 178° angle at nitrogen), whereas the shortest corresponds to a highly nonlinear cyanide coordination (with a 139° angle at nitrogen). The remaining $[\text{Os}(\text{phen})(\text{CN})_4]^{2-}$ unit [based on Os(3)] acts as an isolated counterion, with all four of its cyanide groups forming CN···HOH hydrogen bonds with lattice water molecules.

It is apparent that the main difference between this structure and the previous one, both of which are formed from the same components, is that each Ln(III) center in the **Os–Ln–PhenB** structural type is coordinated to only one phen ligand, whereas in the previous structure (**Os–Ln–PhenA**, the discrete hexanuclear assembly), each Ln(III) center is coordinated to two phen ligands, limiting the possibilities for forming higher-dimensional assemblies via additional cyanide bridges. This difference occurs despite the fact that in both cases 2 equiv of phen was used in the crystallization mixture.

The next two types of structure arise from crystallization of $\text{Na}_2[\text{Os}(\text{phen})(\text{CN})_4]$ and a Ln(III) nitrate salt in the presence of bpym. The first type is a one-dimensional “chain of squares”, exemplified by the structure of $\{[\text{Os}(\text{phen})(\text{CN})_4]_3[\text{Er}(\text{H}_2\text{O})_3]_2[\text{Er}(\text{H}_2\text{O})_4](\text{bpym})(\text{H}_2\text{O})_{13}(\text{MeOH})\}_\infty$ (**Os–Er–BpymA**), which is shown in Figures 6 and 7. The structure is based on square $\text{Os}_2\text{Er}_2(\mu\text{-CN})_4$ units that incorporate two crystallographically independent $[\text{Os}(\text{phen})(\text{CN})_4]^{2-}$ units and two Er(III) ions. Each $[\text{Os}(\text{phen})(\text{CN})_4]^{2-}$ unit uses the pair of cyanide ligands in the same plane as the phen ligand (i.e., its equatorial pair) to coordinate to the two Er(III) ions. Adjacent $\text{Os}_2\text{Er}_2(\mu\text{-CN})_4$ squares are connected by a bridging bipyrimidine ligand which coordinates to one Er(III) ion of each Os_2Er_2 square, forming a $\cdots\{\text{Os}_2\text{Er}_2\}(\mu\text{-bpym})\{\text{Os}_2\text{Er}_2\}(\mu\text{-bpym})\cdots$ sequence (Figure 7). Both of the Er(III) ions are eight-coordinate. Er(1) is coordinated by two bridging cyanides, a bidentate bpym ligand, and four water molecules; Er(2) has only three water molecules, and its eighth site is filled by a cyanide ligand from an additional $[\text{Os}(\text{phen})(\text{CN})_4]^{2-}$ unit that is pendent from the backbone of the chain. Thus, the repeat unit of the chain is a pentanuclear Os_3Er_2 fragment (Figure 6). As in the other structures, those cyanide groups which are not coordinated to Er(III) are involved in CN···HOH hydrogen-bonding interactions with lattice water molecules. The related Yb(III) complex is isostructural, but the structural determination was of much poorer quality and thus was not included here.

The second type of structure arising from this combination of components is exemplified by $\{[\text{Os}(\text{phen})(\text{CN})_4]_6[\text{Nd}(\text{H}_2\text{O})_2][\text{Nd}(\text{H}_2\text{O})_3][\text{Nd}(\text{H}_2\text{O})_4][\text{Nd}(\text{H}_2\text{O})_3(\text{MeOH})](\text{bpym})_2(\text{MeOH})_6(\text{H}_2\text{O})_{19.5}\}_\infty$ (**Os–Nd–BpymB**), in which $[\text{Os}(\text{phen})(\text{CN})_4]^{2-}$ units, Nd(III) ions, and bpym ligands combine in a 3:2:1 ratio in a two-dimensional polymeric structure (Figures 8 and 9). The asymmetric unit (Figure 8) contains six independent Os(II) and four independent Nd(III) centers; these are arranged into two-dimensional layers having a rather complicated structure (Figure 9).

Table 2. Crystal Parameters and Data Collection and Refinement Details for the Structures in This Paper

complex	$\{[\text{Os}(\text{phen})(\text{CN})_4]_1,5^-[\text{Gd}(\text{H}_2\text{O})_4^+(\text{MeOH})](\text{H}_2\text{O})_4\}_\infty$	$\text{Na}_2\{[\text{Os}(\text{phen})-(\text{CN})_4]_4[\text{Pr}(\text{phen})_2-(\text{H}_2\text{O})_2]\} \cdot 4\text{MeOH} \cdot 17\text{H}_2\text{O}$	$\text{Na}_2\{[\text{Os}(\text{phen})-(\text{CN})_4]_4[\text{Nd}(\text{phen})_2-(\text{H}_2\text{O})_2]\} \cdot 2\text{MeOH} \cdot 21\text{H}_2\text{O}$	$\text{Na}_2\{[\text{Os}(\text{phen})-(\text{CN})_4]_4[\text{Gd}(\text{phen})_2-(\text{H}_2\text{O})_2]\} \cdot 21\text{H}_2\text{O}$	$\text{Na}_2\{[\text{Os}(\text{phen})-(\text{CN})_4]_4[\text{Er}(\text{phen})_2-(\text{H}_2\text{O})_2]\} \cdot 4\text{MeOH} \cdot 20\text{H}_2\text{O}$	$\text{Na}_2\{[\text{Os}(\text{phen})-(\text{CN})_4]_4[\text{Yb}(\text{phen})_2-(\text{H}_2\text{O})_2]\} \cdot 20\text{H}_2\text{O}$
abbreviation	Os–Gd	Os–Pr–PhenA	Os–Nd–PhenA	Os–Gd–PhenA	Os–Er–PhenA	Os–Yb–PhenA
formula	$\text{C}_{50}\text{H}_{64}\text{Gd}_2\text{N}_{18}\text{O}_{18}\text{Os}_3$	$\text{C}_{116}\text{H}_{118}\text{N}_{32}\text{Nd}_2\text{O}_{25}\text{Os}_4$	$\text{C}_{114}\text{H}_{118}\text{N}_{32}\text{Nd}_2\text{O}_{23}\text{Os}_4$	$\text{C}_{116}\text{H}_{110}\text{Gd}_2\text{N}_{32}\text{Nd}_2\text{O}_{23}\text{Os}_4$	$\text{C}_{116}\text{H}_{124}\text{Er}_2\text{N}_{32}\text{Na}_2\text{O}_{26}\text{Os}_4$	$\text{C}_{119}\text{H}_{108}\text{N}_{32}\text{Na}_2\text{O}_{22}\text{Os}_4\text{Yb}_2$
mol wt	2090.29	3417.02	3431.66	3393.60	3523.77	3407.16
<i>T</i> (K)	150(2)	100(2)	100(2)	120(2)	100(2)	150(2)
cryst syst	orthorhombic	monoclinic	monoclinic	monoclinic	monoclinic	monoclinic
space group	<i>Pbcn</i>	<i>P2₁/c</i>	<i>P2₁/c</i>	<i>P2₁/c</i>	<i>P2₁/c</i>	<i>P2₁/c</i>
<i>a</i> (Å)	14.858(3)	14.3807(15)	14.3528(11)	14.266(2)	14.1699(18)	14.1796(11)
<i>b</i> (Å)	30.492(5)	27.939(3)	27.880(2)	27.920(5)	27.810(4)	27.713(2)
<i>c</i> (Å)	13.530(2)	17.3682(19)	17.3744(13)	17.365(3)	17.237(3)	17.1951(13)
α (deg)	90	90	90	90	90	90
β (deg)	90	100.375(6)	100.908(4)	101.780(11)	101.968(7)	101.828(5)
γ (deg)	90	90	90	90	90	90
<i>V</i> (Å ³)	6129.8(18)	6864.1(12)	6827.0(9)	6771(2)	6644.7(16)	6613.6(9)
<i>Z</i>	4	2	2	2	2	2
ρ (g cm ⁻³)	2.265	1.653	1.669	1.665	1.761	1.711
cryst size (mm ³)	$0.20 \times 0.20 \times 0.04$	$0.43 \times 0.31 \times 0.22$	$0.26 \times 0.20 \times 0.10$	$0.27 \times 0.12 \times 0.06$	$0.34 \times 0.18 \times 0.08$	$0.15 \times 0.06 \times 0.06$
μ (mm ⁻¹)	8.415	4.464	4.537	4.784	5.144	5.308
data, restraints, params	10280, 0, 413	12071, 14, 831	12008, 0, 848	11849, 18, 829	11674, 0, 840	11628, 18, 823
final <i>R</i> ₁ , w <i>R</i> ₂	0.0225, 0.0424	0.0386, 0.1282	0.0352, 0.1137	0.0429, 0.1488	0.0338, 0.1010	0.0613, 0.1738
complex	$\{[\text{Os}(\text{phen})(\text{CN})_4]_3^-[\text{Pr}(\text{H}_2\text{O})_2^-(\text{phen})]_2(\text{H}_2\text{O})_{10,5}\}_\infty$	$\{[\text{Os}(\text{phen})(\text{CN})_4]_3^-[\text{Nd}(\text{H}_2\text{O})_2^-(\text{phen})]_2(\text{H}_2\text{O})_{10,5}\}_\infty$	$\{[\text{Os}(\text{phen})(\text{CN})_4]_3^-[\text{Er}(\text{H}_2\text{O})_3^-(\text{H}_2\text{O})_{13}(\text{bpyym})_2^-(\text{MeOH})_6(\text{H}_2\text{O})_{19,5}\}_\infty$	$\{[\text{Os}(\text{phen})(\text{CN})_4]_6[\text{Nd}_4(\text{H}_2\text{O})_{12}^-(\text{MeOH})(\text{bpyym})_2^-(\text{MeOH})_6(\text{H}_2\text{O})_{19,5}\}_\infty$	$\{[\text{Os}(\text{phen})(\text{CN})_4]_6[\text{Pr}_4^-(\text{H}_2\text{O})_{13}(\text{bpyym})_2^-(\text{MeOH})(\text{H}_2\text{O})_{25}\}_\infty$	
abbreviation	Os–Pr–PhenB	Os–Nd–PhenB	Os–Er–BpymB	Os–Nd–BpymB	Os–Pr–BpymB	
formula	$\text{C}_{72}\text{H}_{71}\text{N}_{22}\text{O}_{15,5}\text{Os}_3\text{Pr}_2$	$\text{C}_{72}\text{H}_{69}\text{N}_{22}\text{Nd}_2\text{O}_{14,5}\text{Os}_3$	$\text{C}_{57}\text{H}_{74}\text{Er}_2\text{N}_{22}\text{O}_2\text{Os}_3$	$\text{C}_{119}\text{H}_{151}\text{N}_{44}\text{Nd}_4\text{O}_{38,5}\text{Os}_6$	$\text{C}_{113}\text{H}_{140}\text{N}_{44}\text{O}_{39}\text{Os}_6\text{Pr}_4$	
mol wt	2344.93	2333.57	2308.50	4532.00	4443.53	
<i>T</i> (K)	100(2)	100(2)	100(2)	100(2)	150(2)	
cryst syst	triclinic	triclinic	triclinic	monoclinic	monoclinic	
space group	<i>P1</i>	<i>P1</i>	<i>P1</i>	<i>P2₁/n</i>	<i>P2₁/n</i>	
<i>a</i> (Å)	10.971(12)	10.9539(6)	15.4500(9)	20.2500(11)	20.1983(11)	
<i>b</i> (Å)	17.303(18)	17.9486(11)	15.7773(9)	27.4569(16)	27.4911(16)	
<i>c</i> (Å)	22.09(2)	22.4030(14)	17.6472(10)	27.5852(16)	27.6564(16)	
α (deg)	72.965(10)	74.954(4)	111.210(3)	90	90	
β (deg)	80.75(3)	82.143(3)	95.676(3)	90.310(3)	90.327(3)	
γ (deg)	84.799(17)	84.232(3)	95.219(3)	90	90	
<i>V</i> (Å ³)	3953(8)	4203.9(4)	3953.2(4)	15337.2(15)	15.356.6(15)	
<i>Z</i>	2	2	2	4	4	
ρ (g cm ⁻³)	1.970	1.844	1.939	1.963	1.922	
cryst size (mm ³)	$0.23 \times 0.15 \times 0.05$	$0.28 \times 0.06 \times 0.05$	$0.42 \times 0.14 \times 0.04$	$0.46 \times 0.17 \times 0.12$	$0.26 \times 0.05 \times 0.04$	
μ (mm ⁻¹)	6.092	5.803	6.982	6.363	6.270	
data, restraints, params	13804, 18, 1061	12991, 42, 1073	13829, 30, 993	27012, 6, 1883	27038, 55, 1851	
final <i>R</i> ₁ , w <i>R</i> ₂	0.0314, 0.0772	0.0424, 0.1116	0.0549, 0.1631	0.0450, 0.1026	0.0612, 0.1472	

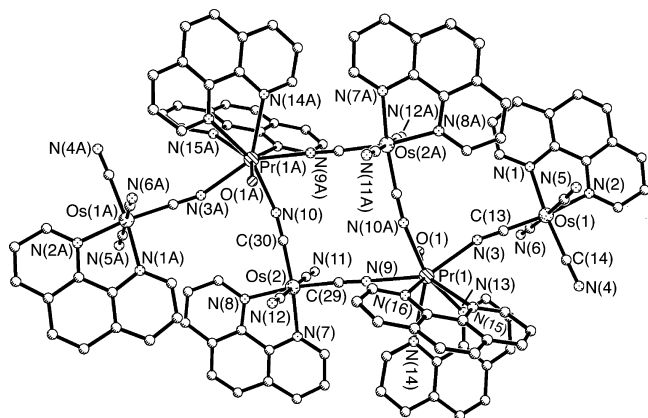


Figure 3. Structure of the hexanuclear Os_4Pr_2 anionic cluster in the structure of **Os-Pr-PhenA**. The two equivalent halves are related by an inversion center. H atoms and lattice solvent molecules have been omitted for clarity.

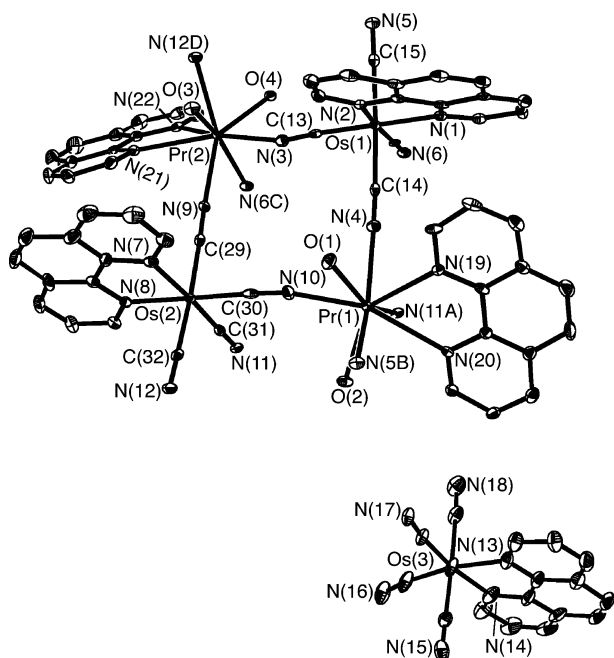


Figure 4. ORTEP view of the asymmetric unit of **Os-Pr-PhenB**. H atoms and lattice solvent molecules have been omitted for clarity. A few extra atoms from adjacent asymmetric units have been added in order to complete the coordination spheres around the metal ions.

The “top” and “bottom” of each layer consist of the phenanthroline ligands of $[\text{Os}(\text{phen})(\text{CN})_4]^{2-}$ units, whose cyanide ligands are directed inward; the polar center of the layer contains the Nd(III) centers, bridging bpym ligands, and water molecules. Figure 9a shows a view of the central part of a layer, namely, the Os–CN–Nd network and the bridging bipyrimidine ligands (the water ligands have been removed for clarity). The two bipyrimidine ligands each bridge a pair of Nd(III) centers [Nd(1)/Nd(2) and Nd(3)/Nd(4)] and form portions of heptametallic ring assemblies consisting of the cyclic sequence {Nd(1)–Os(4)–Nd(4)–(bpym)–Nd(3)–Os(2)–Nd(2)–(bpym)–} plus an additional $[\text{Os}(\text{phen})(\text{CN})_4]^{2-}$ unit [Os(6)] that spans both Nd(1) and Nd(2). These heptametallic units are linked by smaller $\text{Os}_2\text{Nd}_2(\mu\text{-CN})_4$ tetrametallic rings consisting of the sequence {Nd(1)–

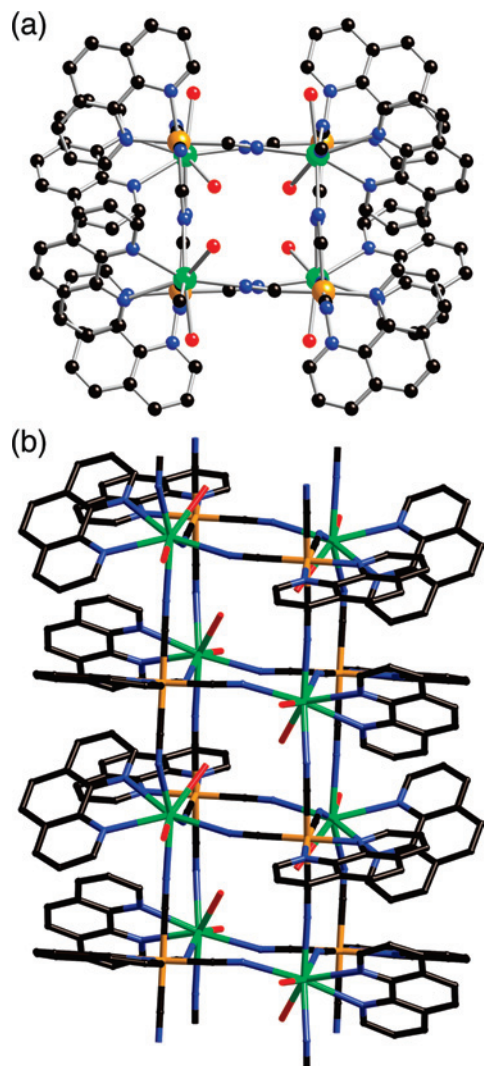


Figure 5. Two mutually perpendicular views of a “tube” in the structure of **Os-Pr-PhenB**: (a) a top view looking down into a tube; (b) a side view of a tube. (Color key: Pr, green; Os, orange; C, black; N, blue; O, red.)

Os(3)–Nd(3′)–Os(1)–}. The result is an alternating one-dimensional sequence of heptametallic and tetrametallic rings (running from bottom left to top right in Figure 9b) in which Nd(1) and Nd(3) are common to both ring structures. The remaining $[\text{Os}(\text{phen})(\text{CN})_4]^{2-}$ units [Os(5)] cross-link these one-dimensional chains via cyanide bridges to Nd(4) in one chain and Nd(2) in an adjacent one. The Pr(III) analogue is isostructural.

Photophysical Properties. In previous work,⁷ we showed that the MLCT absorptions of $[\text{Os}(\text{diimine})(\text{CN})_4]^{2-}$ complexes (comprising both ¹MLCT absorptions at higher energy and a ³MLCT absorption at lower energy) are not only solvatochromic but also metallochromic, that is, coordination of the cyanide N atoms to additional metal cations such as Ba^{2+} or Na^+ results in a substantial blue shift of the MLCT absorption manifold and the ³MLCT luminescence. As in the case of the well-known solvatochromism of the Ru(II) analogues,¹⁰ this effect arises from stabilization of the $d(\pi)$ orbital set when an electron-withdrawing group is attached to the cyanide N atoms, making the cyanide ligands stronger π acceptors with respect to the Os(II) center. Thus, in MeCN,

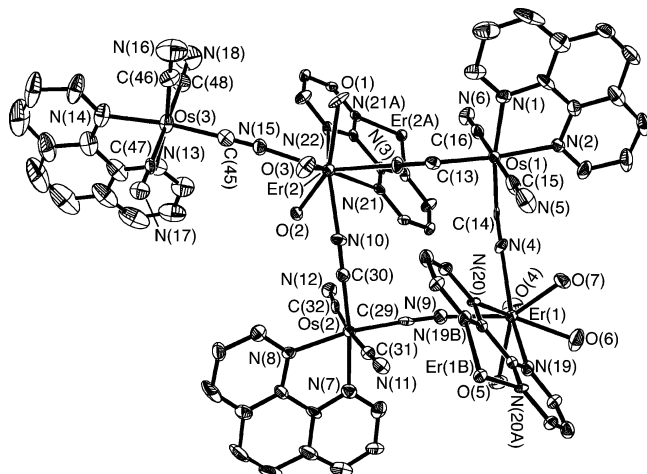


Figure 6. ORTEP view of the asymmetric unit of **Os–Er–BpymA**. H atoms and lattice solvent molecules have been omitted for clarity. A few extra atoms from adjacent asymmetric units have been added in order to show the complete coordination of the bipyrimidine ligands, each of which spans two Er(III) centers.

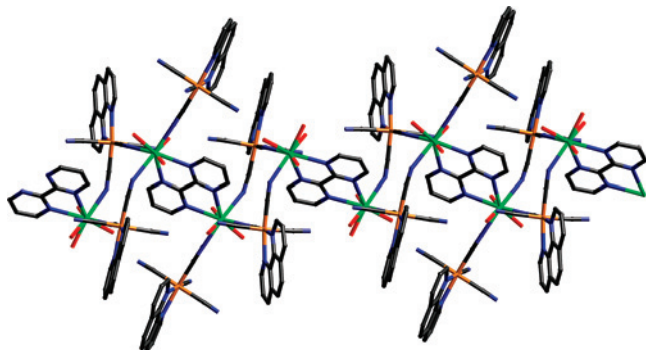


Figure 7. View of the one-dimensional “chain of squares” in the structure of **Os–Er–BpymA**. (Color key: Er, green; Os, orange; C, black; N, blue; O, red.)

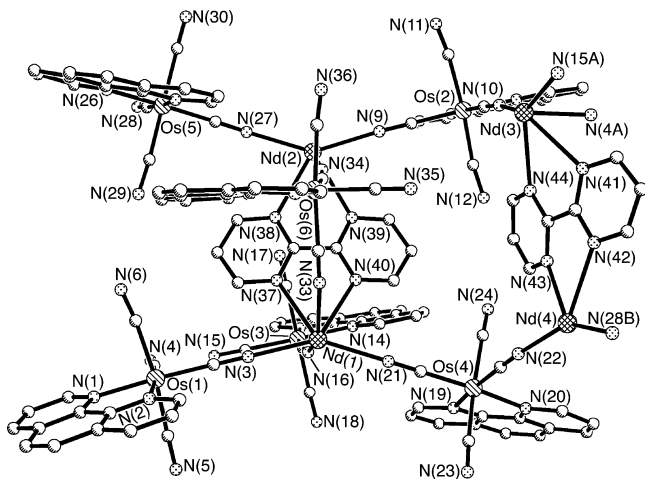


Figure 8. ORTEP view of the asymmetric unit of **Os–Nd–BpymB**. H atoms and lattice solvent molecules have been omitted for clarity. A few extra atoms from adjacent asymmetric units have been added in order to complete the coordination spheres around the metal ions.

the $^3\text{MLCT}$ and two $^1\text{MLCT}$ absorptions of $[\text{Os}(\text{Bu}_2\text{bipy})(\text{CN})_4]^{2-}$ ($\text{Bu}_2\text{bipy} = 4,4'$ -di-*tert*-butyl-2,2'-bipyridine) occur at 705, 544, and 377 nm, respectively. In the presence of a soluble Ba^{2+} salt, the $^3\text{MLCT}$ and lower-energy $^1\text{MLCT}$ bands are blue-shifted to 530 and 425 nm, respectively, and

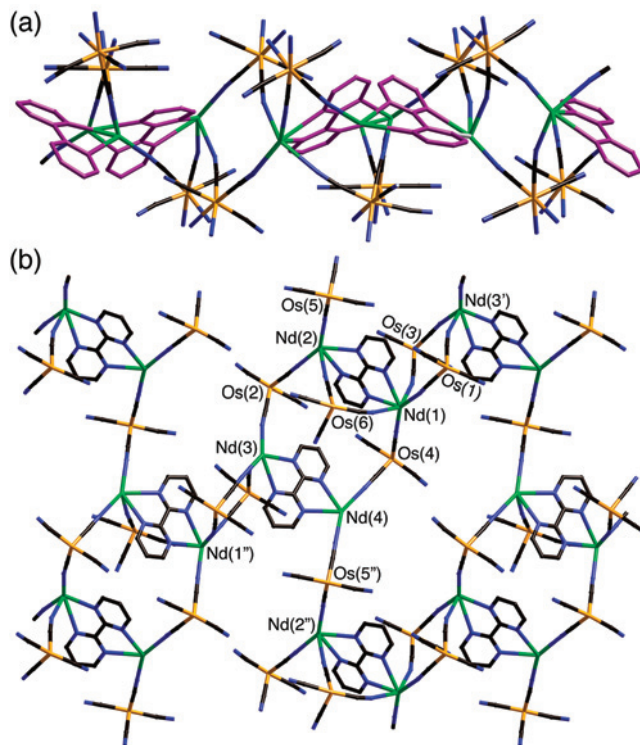


Figure 9. Two mutually perpendicular views of one of the two-dimensional sheets in the structure of **Os–Nd–BpymB**: (a) an edge-on view, with the phenanthroline C atoms not shown and the bpy ligands shown in purple; (b) a face-on view, with the phenanthroline ligands completely omitted. In both views, water ligands have been omitted for clarity. (Color key: Nd, green; Os, orange; C, black; N, blue.)

the higher-energy $^1\text{MLCT}$ absorption is blue-shifted far enough to become obscured by $\pi-\pi^*$ transitions in the UV region. Likewise, the $^3\text{MLCT}$ luminescence in the presence of Ba^{2+} ions is blue-shifted from 970 to 685 nm and strengthened from a vanishingly weak emission to a much more intense one having a lifetime of ~ 85 ns.⁷

In the crystal structures described in this paper, the coordination environment around the $[\text{Os}(\text{phen})(\text{CN})_4]^{2-}$ unit is comparable to that found in the presence of excess Ba^{2+} ions in a noncompetitive solvent, i.e., with many of the cyanide N atoms directly coordinated to electropositive metal ions. We therefore expect the MLCT absorption and emission spectra of the Os(II) center to be at the high-energy extremes of the accessible ranges. An absorption spectrum of **Os–Gd–PhenA** (measured by reflectance on a powdered crystalline sample) confirmed this, exhibiting a broad absorption band in the visible region with a maximum at ~ 430 nm and a lower-energy shoulder at 530 nm; this result is similar to what was observed for $[\text{Os}(\text{Bu}_2\text{bipy})(\text{CN})_4]^{2-}/\text{Ba}^{2+}$ in MeCN solution, where the visible region was dominated by the lower-energy $^1\text{MLCT}$ absorption at 425 nm. The resulting Os(II)-based $^3\text{MLCT}$ luminescence from **Os–Gd–PhenA** occurred as a broad band with an (uncorrected) maximum at 680 nm and a lifetime of 67 ns (Figure 10). In these complexes, the Gd(III) ion cannot quench the Os(II)-based luminescence either by energy transfer (as its lowest

(10) (a) Ward, M. D. *Coord. Chem. Rev.* **2006**, *250*, 3128. (b) Timpon, C. J.; Bignozzi, C. A.; Sullivan, B. P.; Kober, E. M.; Meyer, T. J. *J. Phys. Chem.* **1996**, *100*, 2915.

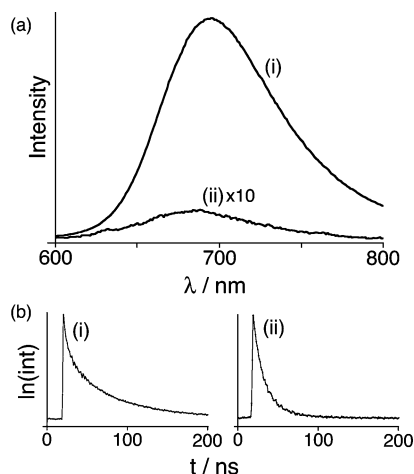


Figure 10. (a) Steady-state emission spectra of Os(II)-based luminescence in **Os–Gd–PhenA** [unquenched, curve (i)] and **Os–Er–PhenA** [partially quenched by energy transfer, curve (ii)]; the intensity of this spectrum has been multiplied by a factor of 10. (b) Time-resolved emission decays from the same two samples, giving Os(II)-based lifetimes of 67 ns for **Os–Gd–PhenA** and 7 ns (major component) for **Os–Er–PhenA**.

f–f excited state lies in the UV region) or by electron transfer, so this represents the highest possible luminescence intensity and lifetime of the $[\text{Os}(\text{phen})(\text{CN})_4]^{2-}$ unit in this crystalline environment. There was no resolved fine structure in the emission profile, so the position of the highest-energy 0–0 component was not clear; however, from the onset of the luminescence at the high-energy side of the curve, we estimated the ${}^3\text{MLCT}$ energy to be $\sim 16\,000\text{ cm}^{-1}$. Very similar results were obtained for the Os(II)-based luminescence from **Os–Gd** ($\lambda_{\text{em}} = 662\text{ nm}$, $\tau = 80\text{ ns}$) and **Os–Gd–BpymB** ($\lambda_{\text{em}} = 669\text{ nm}$, $\tau = 75\text{ ns}$).

The series of complexes **Os–Ln–PhenA** (Ln = Pr, Nd, Er, Yb) was also examined. All of the Ln(III) ions in this series have low-energy f–f states capable of displaying near-infrared luminescence and thereby quenching the Os(II) centers by $\text{Os} \rightarrow \text{Ln}$ energy transfer across the cyanide bridges. We concentrated our studies on this series because all of its members had been structurally characterized and found to be isostructural, with all of the $[\text{Os}(\text{phen})(\text{CN})_4]^{2-}$ units connected to Ln(III) centers via cyanide bridges and therefore able to participate in any energy transfer processes.¹¹

In the visible region, the members of this series of complexes all showed residual Os(II)-based luminescence

(11) The other series are not unambiguously complete in the same way and therefore cannot be used for comparison of different members of an isostructural series. For the **Os–Ln** series, only **Os–Gd** could be structurally characterized; the other members did not form single crystals, possibly because they are of a different structural type. For the **Os–Ln–Bpym** series, only two members of structural type **A** and three of type **B** could be isolated as analytically pure crystalline solids (see the Experimental Section). The structures of the members of the **Os–Ln–PhenB** series (Figure 4) contain some $[\text{Os}(\text{phen})(\text{CN})_4]^{2-}$ units that are connected to Ln(III) centers and some that are not. This leads to different degrees of quenching for different Os(II) units in the same crystal, considerably complicating any photophysical analysis based on measuring residual Os(II)-based emission in the presence of different Ln(III) ions. The **Os–Ln–PhenA** series is (i) complete, (ii) isostructural, and (iii) devoid of “free” Os(II) units that are not connected to Ln(III) centers; thus, it is an ideal basis for a systematic comparison of photophysical properties.

Table 3. Summary of Photophysical Data for the Series of Isostructural **Os–Ln–PhenA** Complexes

complex	$\lambda_{\text{em}}(\text{Os}, {}^3\text{MLCT})$ (nm) ^a	$\tau_{\text{q}}(\text{Os})$ (ns) ^b	$\tau(\text{Ln})$ (ns) ^c
Os–Pr–PhenA	678	25	–
Os–Nd–PhenA	688	<2	90, 360 ^d
Os–Er–PhenA	679	7	~ 70 ^e
Os–Yb–PhenA	675	8	670 ^f

^a Emission maxima are uncorrected. ^b Obtained using 405 nm excitation into the MLCT absorption manifold. ^c Obtained using 532 nm excitation into the MLCT absorption manifold. ^d Measured at both 1055 and 1340 nm; dual exponential. ^e Measured at 1530 nm; very weak. ^f Measured at 975 nm.

located at the same wavelength as that from **Os–Gd–PhenA** but having much lower intensity (>90% quenched in all cases, as shown in Figures 10 and 12). This may arise from incomplete quenching by the Ln(III) ions to which the $[\text{Os}(\text{phen})(\text{CN})_4]^{2-}$ units are attached and also from inhomogeneities/defect sites in the crystals that cause some unquenched $[\text{Os}(\text{phen})(\text{CN})_4]^{2-}$ chromophores to be present.^{1a} This was confirmed by time-resolved measurements on the solid materials, which in every case except for **Os–Nd–PhenA** showed a dual-exponential luminescence decay. The minor, longer-lived component arose from unquenched $[\text{Os}(\text{phen})(\text{CN})_4]^{2-}$ chromophores, as shown by the lifetime of $\sim 70\text{ ns}$ in each case. The dominant component, however, was much shorter lived and corresponds to the residual emission from the partially quenched $[\text{Os}(\text{phen})(\text{CN})_4]^{2-}$ units following $\text{Os} \rightarrow \text{Ln}$ energy transfer (e.g., see Figure 10b). These shorter Os(II)-based lifetimes, $\tau_{\text{q}}(\text{Os})$, which are summarized along with the other photophysical data in Table 3, were (in order of quenching) 25, 8, and 7 ns for the Pr(III), Yb(III) and Er(III) adducts, respectively, and undetectably short (<2 ns) for the Nd(III) adduct, for which only a weak 70 ns component from unquenched $[\text{Os}(\text{phen})(\text{CN})_4]^{2-}$ chromophores could be detected. From these results, using eq 1 and taking the lifetime of 67 ns for the Gd(III) adduct as the “unquenched” lifetime (τ_{u}), we obtained $\text{Os} \rightarrow \text{Ln}$ energy transfer rates (k_{ET}) of 2.5×10^7 , 1.1×10^8 , 1.3×10^8 , and $>5 \times 10^8\text{ s}^{-1}$ for Pr(III), Yb(III), Er(III), and Nd(III), respectively.

$$k_{\text{ET}} = \frac{1}{\tau_{\text{q}}} - \frac{1}{\tau_{\text{u}}} \quad (1)$$

The following discussion makes use of the energy-level diagram for the Ln(III) ions that is shown in Figure 11. It is not surprising that Nd(III) is the most effective energy acceptor, as is commonly observed in d–f donor/acceptor systems based on transition-metal chromophores whose energy content causes them to luminesce in the visible region. This arises because Nd(III) has the highest density of f–f states at energies that overlap with typical luminescence profiles of the d-block units.⁹ Nd(III) has several excited states that overlap with the Os(II)-based emission profile, starting with the ${}^4\text{F}_{3/2}$ level at $11\,500\text{ cm}^{-1}$ and including several other states with energies ranging from just above this one up to the Os(II)-based ${}^3\text{MLCT}$ energy. This gives a greater spectroscopic overlap between the emission of the donor and the absorption of Nd(III) compared with those of the other Ln(III) ions, resulting in the fastest energy transfer ($k_{\text{ET}} > 5 \times 10^8\text{ s}^{-1}$) for this series. The emissive ${}^4\text{F}_{3/2}$ level

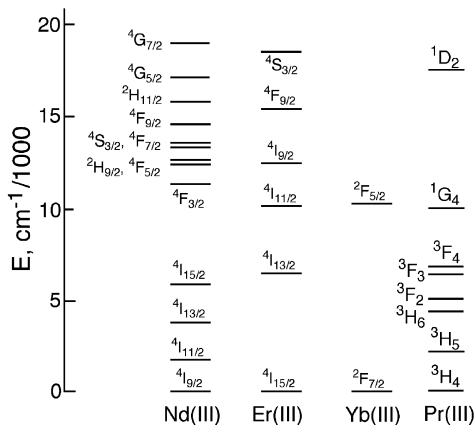


Figure 11. Energy levels of Pr(III), Nd(III), Er(III), and Yb(III).

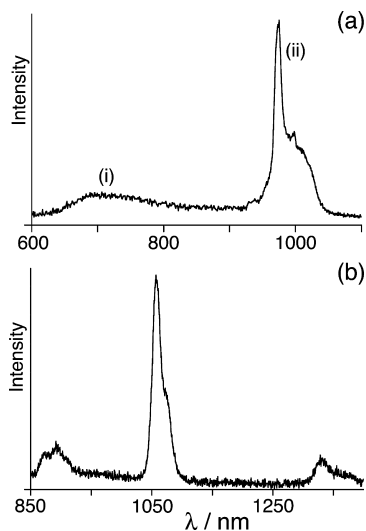


Figure 12. Emission spectra of (a) Os–Gd–PhenA and (b) Os–Nd–PhenA following excitation into the Os(II)-based MLCT absorption manifold at 532 nm. In each case, the sensitized Ln(III)-based emission is clear. For (a), note the weak residual Os(II)-based emission [component (i)] in addition to the Yb(III)-based emission [component (ii)].

should not itself be able to act as an energy acceptor because the $4F_{3/2} \leftarrow 4I_{9/2}$ transition has $|\Delta J| = 3$, which is formally forbidden by both the Förster and Dexter mechanisms;¹² however, this restriction does not apply to the several f–f states which lie close above this.

It is noteworthy that this energy transfer is also faster than that observed for an analogous [Ru(bipy)(CN)₄]²⁻/Nd(III) system, in which Ru(II) → Nd(III) energy transfer occurred with a rate constant of $2 \times 10^8 \text{ s}^{-1}$.^{1a} This difference may be ascribed to better spectroscopic overlap between the lower-lying Os(II)-based ³MLCT emission and the f–f absorptions of Nd(III) lying in the 11 500–16 000 cm⁻¹ range. It is also possible that increased Os(II)–Nd(III) electronic coupling across the cyanide bridge may occur because of the greater spatial extension of the 5d orbitals of

Os(II) compared to that of the 4d orbitals of Ru(II); such enhanced coupling can further facilitate any energy transfer that occurs via the Dexter mechanism.³

In the same way, the Os → Yb energy transfer observed here is also much faster than the Ru(II) → Yb(III) energy transfer found in an [Ru(bipy)(CN)₄]²⁻/Yb(III) adduct.^{1a} In that case, relatively poor spectroscopic overlap between the higher-energy Ru(II)-based emission (having a ³MLCT energy of $\sim 20\,000 \text{ cm}^{-1}$) and the Yb(III) f–f level at $10\,200 \text{ cm}^{-1}$ resulted in rather slow Ru(II) → Yb(III) energy transfer ($k_{\text{ET}} \approx 3 \times 10^6 \text{ s}^{-1}$).^{1a} In contrast, the Os(II) → Yb(III) energy transfer observed here ($k_{\text{ET}} = 1.1 \times 10^8 \text{ s}^{-1}$) is nearly 2 orders of magnitude faster over essentially the same distance, for the same combination of reasons: better donor/acceptor overlap arising from a better match between the lower energy of the Os(II) donor and the Yb(III) f–f level, along with possibly increased Os(II)–Yb(III) electronic coupling because of the greater spatial extension of the 5d orbitals of Os(II). In this system, the Dexter mechanism for energy transfer necessarily applies, given that $|\Delta J| = 1$ for a transition between the ground and excited f–f levels of Yb(III).¹²

A similar situation pertains with Er(III), for which the four possible energy-accepting levels are, in order of increasing energy, the luminescent $4I_{13/2}$ level at 6500 cm^{-1} and the $4I_{11/2}$, $4I_{9/2}$, and $4F_{9/2}$ levels above this (the $4F_{9/2}$ level lies at $\sim 15\,500 \text{ cm}^{-1}$). On the basis of the known selection rules for energy transfer to lanthanides, excitations from the ground state ($4I_{15/2}$) to the $4I_{9/2}$ or $4F_{9/2}$ levels, both of which require $|\Delta J| = 3$, are not permitted by either the Förster or Dexter mechanisms.¹² The involvement of these levels can therefore be ruled out to a first approximation, although it should be remembered that these selection rules apply only to the extent that J is a good quantum number and are further relaxed by mixing of forbidden 4f–4f transitions with allowed 4f–5d transitions.¹³ This leaves the two lowest excited levels of Er(III) ($4I_{13/2}$ and $4I_{11/2}$) to act as the main energy acceptors, since transitions from the ground state to these levels (with respective $|\Delta J|$ values of 1 and 2) are allowed by the Dexter and Förster mechanisms, respectively.¹² Given their low energies of 6500 and $10\,000 \text{ cm}^{-1}$ respectively, it is again apparent that reducing the ³MLCT energy of the donor [in going from Ru(II) to Os(II)] results in a better energy match and improved spectroscopic overlap with these f–f states, accounting for the much faster Os(II) → Er(III) energy transfer ($k_{\text{ET}} = 1.3 \times 10^8 \text{ s}^{-1}$) compared with Ru(II) → Er(III) energy transfer (10^7 s^{-1}) across the same distance and the same bridging ligand. Again, increased metal–metal electronic coupling due to the greater extension of the Os(II) 5d orbitals is also feasible.

Os(II) → Pr(III) energy transfer is the slowest by a significant margin ($k_{\text{ET}} = 2.5 \times 10^7 \text{ s}^{-1}$), although its rate is comparable to the Ru(II) → Pr(III) energy transfer rate that we observed previously in a [Ru(bipy)(CN)₄]²⁻/Pr(III) adduct ($k_{\text{ET}} = 4 \times 10^7 \text{ s}^{-1}$).^{1a} The relatively low ³MLCT energy of the Os(II) donor ($\sim 16\,000 \text{ cm}^{-1}$) cannot populate the $1D_2$

(12) (a) de Sá, G. F.; Malta, O. L.; de Mello Donegá, C.; Simas, A. M.; Longo, R. L.; Santa-Cruz, P. A.; da Silva, E. F. *Coord. Chem. Rev.* **2000**, *196*, 165. (b) Hebbink, G. A.; Grave, L.; Woldering, L. A.; Reinhoudt, D. N.; van Veggel, F. C. J. M. *J. Phys. Chem. A* **2003**, *107*, 2483.

(13) Blasse, G.; Grabmaier, B. C. *Luminescent Materials*; Springer-Verlag: Berlin, 1994.

level of Pr(III) (at $\sim 17\,500\text{ cm}^{-1}$) or anything above it; the highest available f–f state is 1G_4 , which lies just below $10\,000\text{ cm}^{-1}$. This leads to the following question: why is Os(II) \rightarrow Yb(III) energy transfer an order of magnitude faster than Os(II) \rightarrow Pr(III) energy transfer when the intermetallic distances are very similar; the bridging ligand is the same; the energies of the accepting f–f states are comparable ($\sim 10\,000\text{ cm}^{-1}$ in each case); and the energy transfer mechanisms should also be the same in each case, given that the $|\Delta E|$ values for transitions to the excited states in Pr(III) and Yb(III) are 0 and 1, respectively, which are consistent only with the Dexter mechanism for energy transfer?¹² A possible reason for this may be the much higher intensity of the relevant f–f absorption for Yb(III) compared with that for Pr(III). For aqueous $\text{Pr}(\text{NO}_3)_3 \cdot 6\text{H}_2\text{O}$, the $^1G_4 \leftarrow ^3H_4$ absorption at 1020 nm has an extinction coefficient of $0.23\text{ M}^{-1}\text{ cm}^{-1}$ (as measured by us); for $\text{Yb}(\text{NO}_3)_3 \cdot 6\text{H}_2\text{O}$, the $^2F_{5/2} \leftarrow ^2F_{7/2}$ absorption at 975 nm is an order of magnitude more intense, with an extinction coefficient of $2.1\text{ M}^{-1}\text{ cm}^{-1}$. This affords improved donor/acceptor spectroscopic overlap in the Os(II)/Yb(III) complex compared with that in the Os(II)/Pr(III) complex, which is crucial for nonradiative energy transfer.

Quenching of the Os(II)-based emission for Ln = Nd and Yb was accompanied by the appearance of sensitized luminescence from the Ln(III) center at the characteristic wavelength in the near-IR region; representative sensitized emission spectra are shown in Figure 12 [note the residual Os(II)-based emission at $\sim 700\text{ nm}$ in Figure 12a, in addition to the sensitized Yb(III)-based emission at 980 nm]. Following excitation into the Os(II)-based MLCT absorption manifold at 532 nm, the lifetime of the sensitized Ln(III)-based emission is short [hundreds of nanoseconds for Yb(III) and tens of nanoseconds for Nd(III)]. This is a general feature of cyanide-bridged coordination networks containing Ln(III) centers¹ that cannot be ascribed to quenching by coordinated OH oscillators because the crystals used in photophysical analysis were grown from deuterated solvents (D_2O and CD_3OD). We believe that the rapid deactivation of the Ln(III)-based excited states arises because of the highly connected network of bridging cyanide ligands. Although CN oscillations occur in the $2000\text{--}2100\text{ cm}^{-1}$ region (comparable to the wavenumber of an O–D vibration) and therefore would not be expected to be particularly effective quenchers of Ln(III) excited states, the formation of an infinite coordination network appears to provide an effective mechanism for phonon-assisted dispersal of the Ln(III)-based excitation energy. In this respect, the presence or absence of additional ancillary ligands (phen, bpym) coordinated to the Ln(III) centers does not have a substantial effect on their photophysical properties, although of course these ligands do play a central role in dictating the structures of the networks.

No sensitized emission was detected from Pr(III), which was to be expected given that the emissive $^1D_2/{}^3P_0$ levels are too high in energy to be populated by energy transfer

from the Os(II) chromophore.¹⁴ Instead, the lower-lying 1G_4 level must be populated, and given the presence of several f–f states just below it, radiative decay from this level was not expected (although near-IR emission originating from the 1G_4 level has been observed in solid-state glasses).¹⁵ Finally, we expected to observe sensitized emission from Er(III) at 1530 nm, arising from the ${}^4I_{13/2}$ level; this luminescence was extremely weak [as is often the case for Er(III)] but just detectable, with a short lifetime ($\sim 70\text{ ns}$).

The **Os–Ln–BpymA** and **Os–Ln–BpymB** samples were also subjected to photophysical study, although the lack of a complete isostructural series means that an analysis similar to the one given above for the **Os–Ln–PhenA** series is not possible.¹¹ However, the available samples showed general behavior similar to that of the **Os–Ln–PhenA** series in the two most important respects: (i) the intensity of the Os(II)-based emission at $\sim 670\text{ nm}$ was substantially reduced for Ln = Yb, Nd, Er, or Pr as opposed to Gd; and (ii) for Ln = Nd, Er, and Yb, weak sensitized luminescence from the relevant Ln(III) ion was observed, with lifetimes of $\sim 300\text{ ns}$ at 980 nm for Yb(III) in **Os–Yb–BpymA**, $\sim 40\text{ ns}$ at 1530 nm for Er(III) in **Os–Er–BpymA**, and $\sim 60\text{ ns}$ at 1060 nm for Nd(III) in **Os–Nd–BpymB**.

Conclusions

$[\text{Os}(\text{phen})(\text{CN})_4]^{2-}$ has been used as a component of cyanide-bridged coordination networks containing Ln(III) cations with additional diimine ligands; several examples have been structurally characterized. In this environment, where the $[\text{Os}(\text{phen})(\text{CN})_4]^{2-}$ units are surrounded by electropositive metal cations, the ${}^3\text{MLCT}$ luminescence of this chromophore occurs at $\sim 680\text{ nm}$ with a lifetime of $\sim 70\text{ ns}$. Ln(III) ions with low-energy f–f states act as energy acceptors and quench the Os(II)-based ${}^3\text{MLCT}$ state, leading to sensitized near-infrared luminescence from Nd(III) and Yb(III) but not from Pr(III); in the latter case, we believe that a nonemissive level is populated. Compared with the situation in related $[\text{Ru}(\text{bipy})(\text{CN})_4]^{2-}/\text{Ln}(\text{III})$ adducts, the reduced energy of the Os(II)-based ${}^3\text{MLCT}$ state results in faster energy transfer to Nd(III), Yb(III), and Er(III) (because of better spectroscopic overlap with the relevant low-energy f–f states of these metal ions) but not to Pr(III) (because the higher-energy luminescent f–f states can no longer participate in energy transfer).

Experimental Section

General Details. Organic ligands and lanthanide salts were purchased from Aldrich and used as received. $\text{Na}_2[\text{Os}(\text{phen})(\text{CN})_4] \cdot 5\text{H}_2\text{O}$ was prepared according to the published method.⁹ Photophysical studies [both steady-state emission spectra and time-resolved measurements of Ln(III) emission in the near-IR region] were performed on ground-up microcrystalline solid samples using a HORIBA Jobin Yvon FluoroLog instrument fitted with a JY TBX

- (14) (a) Voloshin, A. I.; Shavaleev, N. M.; Kazakov, V. P. *J. Lumin.* **2001**, *93*, 199. (b) Davis, G. M.; Aarons, R. J.; Motson, G. R.; Jeffery, J. C.; Adams, H.; Faulkner, S.; Ward, M. D. *Dalton Trans.* **2004**, 1136.
(15) Gu, S. Q.; Turnbull, D. A.; Bishop, S. G. *IEEE Photonics Technol. Lett.* **1996**, *8*, 260.

picosecond photodetection module and a Hamamatsu near-IR R55009-73 detector cooled to $-80\text{ }^{\circ}\text{C}$ using a C9940 housing. Luminescence lifetimes of residual Os(II)-based luminescence in the visible region were measured with an Edinburgh Instruments Mini- τ luminescence lifetime spectrometer equipped with a 405 nm pulsed diode laser excitation source and a cooled Hamamatsu R928 PMT detector; wavelength selection at the detector was accomplished using 50 nm bandpass filters, and for these Os(II) complexes, a 625–675 nm bandpass filter was used.

Syntheses. Detailed synthetic procedures and characterization data are provided below. It should be noted that in many cases the formulations used in calculations of elemental analyses differed from the formulations given in the X-ray crystallographic data in regard to the number of lattice solvent molecules, because extensive disorder caused the determination of the number of lattice solvent molecules from the crystal structures to be highly approximate.

Os–Gd. A hot solution of $\text{Gd}(\text{NO}_3)_3 \cdot 6\text{H}_2\text{O}$ (4.5 mg, 0.01 mmol) in CH_3OH (5 mL) was added to a hot solution of $\text{Na}_2[\text{Os}(\text{phen})(\text{CN})_4] \cdot 5\text{H}_2\text{O}$ (9.2 mg, 0.015 mmol) in water (5 mL). Slow evaporation of the resulting solution afforded red crystals suitable for X-ray diffraction studies in 2–3 weeks. The precipitated crystals were filtered off, washed with water, methanol, and diethyl ether, and dried in air. Yield: 9.5 mg, 90.5%. Anal. Calcd for $\{[\text{Os}(\text{phen})(\text{CN})_4]_{1.5}[\text{Gd}(\text{H}_2\text{O})_4(\text{MeOH})(\text{H}_2\text{O})_4]\}_{\infty}$: C, 28.7; H, 3.1; N, 12.1. Found: C, 28.0; H, 2.6; N, 11.9. IR (KBr pellet): ν (cm^{-1}) 3461 (sh), 3413 (vs, br), 2098 (sh), 2042 (vs), 2030 (sh), 2010 (sh), 1638 (m), 1620 (sh), 1427 (m), 1407 (w), 1384 (m), 1098 (w), 846 (m), 782 (w), 722 (m), 619 (m), 553 (m), 531 (w).

Os–Ln–PhenA (Hexanuclear Clusters). A hot solution of $\text{Ln}(\text{NO}_3)_3 \cdot n\text{H}_2\text{O}$ (0.01 mmol, Ln = Gd, Pr, Nd, Er, Yb) and 1,10-phenanthroline (3.6 mg, 0.02 mmol) in CH_3OH (5 mL) was added to a hot solution of $\text{Na}_2[\text{Os}(\text{phen})(\text{CN})_4] \cdot 5\text{H}_2\text{O}$ (12.1 mg, 0.02 mmol) in water (5 mL). Slow evaporation of the resulting solution afforded crystals suitable for X-ray diffraction studies in 1–2 weeks. Red crystals were separated by filtration, washed with water, methanol, and acetone, and dried in air. Yield: 55–70%.

Data for **Os–Gd–PhenA.** Anal. Calcd for $\text{Na}_2\{[\text{Os}(\text{phen})(\text{CN})_4]_4[\text{Gd}(\text{phen})_2(\text{H}_2\text{O})_2]\}_2 \cdot 23\text{H}_2\text{O}$: C, 39.0; H, 3.4; N, 13.0. Found: C, 38.0; H, 3.0; N, 12.5. IR (KBr pellet): ν (cm^{-1}) 3429 (vs, br), 2098 (sh), 2049 (vs), 2023 (sh), 1626 (m), 1591 (sh), 1577 (sh), 1519 (m), 1496 (sh), 1425 (m), 1384 (sh), 1343 (w), 1142 (w), 1104 (w), 777 (w), 731 (sh), 724 (m), 639 (w), 553 (w).

Data for **Os–Pr–PhenA.** Anal. Calcd for $\text{Na}_2\{[\text{Os}(\text{phen})(\text{CN})_4]_4[\text{Pr}(\text{phen})_2(\text{H}_2\text{O})_2]\}_2 \cdot 24\text{H}_2\text{O}$: C, 39.4; H, 3.4; N, 13.1. Found: C, 38.8; H, 2.9; N, 12.7. IR (KBr pellet): ν (cm^{-1}) 3414 (s, br), 2096 (sh), 2044 (vs), 2015 (sh), 1623 (m), 1591 (sh), 1575 (sh), 1518 (m), 1496 (sh), 1447 (w), 1425 (m), 1384 (m), 1343 (w), 1207 (w), 1142 (w), 1102 (w), 847 (m), 776 (w), 731 (sh), 724 (m), 637 (m), 553 (m).

Data for **Os–Nd–PhenA.** Anal. Calcd for $\text{Na}_2\{[\text{Os}(\text{phen})(\text{CN})_4]_4[\text{Nd}(\text{phen})_2(\text{H}_2\text{O})_2]\}_2 \cdot 25\text{H}_2\text{O}$: C, 39.1; H, 3.5; N, 13.0. Found: C, 38.6; H, 3.1; N, 12.8. IR (KBr pellet): ν (cm^{-1}) 3413 (s, br), 2096 (sh), 2045 (vs), 2014 (sh), 1626 (m), 1590 (sh), 1519 (m), 1495 (sh), 1425 (m), 1384 (m), 1142 (w), 1102 (w), 848 (m), 776 (w), 731 (sh), 724 (m), 638 (m), 553 (m).

Data for **Os–Er–PhenA.** Anal. Calcd for $\text{Na}_2\{[\text{Os}(\text{phen})(\text{CN})_4]_4[\text{Er}(\text{phen})_2(\text{H}_2\text{O})_2]\}_2 \cdot 24\text{H}_2\text{O}$: C, 38.8; H, 3.4; N, 12.9. Found: C, 38.5; H, 3.3; N, 12.4. IR (KBr pellet): ν (cm^{-1}) 3434 (s, br), 2098 (sh), 2053 (vs), 2025 (sh), 1627 (m), 1592 (sh), 1520 (m), 1425 (m), 1384 (m), 1142 (w), 1104 (w), 848 (m), 776 (w), 731 (sh), 724 (m), 639 (w), 554 (w).

Data for **Os–Yb–PhenA.** Anal. Calcd for $\text{Na}_2\{[\text{Os}(\text{phen})(\text{CN})_4]_4[\text{Yb}(\text{phen})_2(\text{H}_2\text{O})_2]\}_2 \cdot 20\text{H}_2\text{O}$: C, 39.5; H, 3.2; N, 13.2.

Found: C, 40.0; H, 2.8; N, 12.9. IR (KBr pellet): ν (cm^{-1}) 3431 (vs, br), 2099 (sh), 2052 (vs), 2026 (sh), 1626 (m), 1592 (sh), 1578 (sh), 1520 (m), 1496 (sh), 1425 (m), 1384 (sh), 1343 (w), 1143 (w), 1105 (w), 865 (sh), 848 (m), 805 (w), 777 (w), 731 (sh), 724 (m), 639 (w), 554 (m).

Os–Ln–PhenB (Tubes). A hot solution of $\text{LnCl}_3 \cdot 6\text{H}_2\text{O}$ (0.01 mmol, Ln = Pr, Nd) and 1,10-phenanthroline (3.6 mg, 0.02 mmol) in CH_3OH (5 mL) was added to a hot solution of $\text{Na}_2[\text{Os}(\text{phen})(\text{CN})_4] \cdot 5\text{H}_2\text{O}$ (9.2 mg, 0.015 mmol) in water (5 mL). Slow evaporation of the resulting solution afforded crystals suitable for X-ray diffraction studies in a few weeks. Red crystals were separated by filtration, washed with water, methanol, and acetone, and dried in air. Yield: 80–90%.

Data for **Os–Pr–PhenB.** Anal. Calcd for $\{[\text{Os}(\text{phen})(\text{CN})_4]_3\text{[Pr}(\text{H}_2\text{O})_2(\text{phen})_2(\text{H}_2\text{O})_{11.5}]\}_{\infty}$: C, 36.9; H, 3.1; N, 13.1. Found: C, 36.8; H, 3.4; N, 12.5. IR (KBr pellet): ν (cm^{-1}) 3429 (s, br), 2096 (sh), 2051 (vs, d), 2044 (vs, d), 2012 (sh), 1624 (m), 1590 (sh), 1576 (sh), 1519 (m), 1425 (m), 1384 (w), 1343 (w), 1142 (w), 1102 (w), 848 (m), 777 (w), 731 (w), 724 (m), 638 (m), 553 (m).

Data for **Os–Nd–PhenB.** Anal. Calcd for $\{[\text{Os}(\text{phen})(\text{CN})_4]_3\text{[Nd}(\text{H}_2\text{O})_2(\text{phen})_2(\text{H}_2\text{O})_{12}]\}_{\infty}$: C, 36.6; H, 3.1; N, 13.2. Found: C, 36.6; H, 2.6; N, 12.6.

Os–Ln–Bpym Complexes (Both Types). A hot solution of $\text{Ln}(\text{NO}_3)_3 \cdot n\text{H}_2\text{O}$ (0.01 mmol, Ln = Gd, Pr, Nd, Er, Yb) and 2,2'-bipyrimidine (3.2 mg, 0.02 mmol) in CH_3OH (5 mL) was added to a hot solution of $\text{Na}_2[\text{Os}(\text{phen})(\text{CN})_4] \cdot 5\text{H}_2\text{O}$ (9.2 mg, 0.015 mmol) in water (5 mL). Slow evaporation of the resulting solution afforded red crystals suitable for X-ray diffraction studies in 2–3 weeks. The precipitated crystals were filtered off, washed with water, methanol, and diethyl ether, and dried in air. Yield: 65–95%.

Data for **Os–Er–BpymA.** Anal. Calcd for $\{[\text{Os}(\text{phen})(\text{CN})_4]_3\text{[Er}(\text{H}_2\text{O})_3\text{[Er}(\text{H}_2\text{O})_4(\text{bpym})(\text{H}_2\text{O})_{15}(\text{MeOH})]\}_{\infty}$: C, 29.2; H, 3.3; N, 13.1. Found: C, 28.8; H, 2.9; N, 12.9. IR (KBr pellet): ν (cm^{-1}) 3436 (s, br), 2103 (sh), 2052 (vs), 2025 (sh), 1630 (m), 1578 (m), 1565 (sh), 1428 (m), 1406 (m), 1384 (m), 1100 (w), 847 (m), 723 (m), 557 (w).

Data for **Os–Yb–BpymA.** Anal. Calcd for $\{[\text{Os}(\text{phen})(\text{CN})_4]_3\text{[Yb}(\text{H}_2\text{O})_3\text{[Yb}(\text{H}_2\text{O})_4(\text{bpym})(\text{H}_2\text{O})_{13}(\text{MeOH})]\}_{\infty}$: C, 29.5; H, 3.2; N, 13.3. Found: C, 29.6; H, 2.7; N, 13.4. IR (KBr pellet): ν (cm^{-1}) 3549 (sh), 3461 (sh), 3414 (s, br), 3237 (sh), 2103 (sh), 2053 (s), 2026 (sh), 1638 (s), 1618 (s), 1583 (sh), 1428 (w), 1407 (w), 1384 (m), 1207 (w), 1147 (w), 847 (w), 781 (w), 757 (w), 723 (w), 624 (m), 480 (m).

Data for **Os–Gd–BpymB.** Anal. Calcd for $\{[\text{Os}(\text{phen})(\text{CN})_4]_6\text{[Gd}(\text{H}_2\text{O})_{13}(\text{bpym})_2(\text{H}_2\text{O})_{29}]\}_{\infty}$: C, 29.6; H, 3.2; N, 13.5. Found: C, 29.2; H, 2.7; N, 13.2. IR (KBr pellet): ν (cm^{-1}) 3543 (sh), 3466 (sh), 3412 (vs, br), 3236 (sh), 2100 (sh), 2048 (m), 2018 (sh), 1638 (m), 1618 (m), 1428 (w), 1408 (w), 1384 (w), 1343 (w), 1201 (w), 1138 (w), 844 (w), 782 (w), 756 (w), 738 (w), 722 (w), 618 (m), 476 (m).

Data for **Os–Pr–BpymB.** Anal. Calcd for $\{[\text{Os}(\text{phen})(\text{CN})_4]_6\text{[Pr}(\text{H}_2\text{O})_{13}(\text{bpym})_2(\text{H}_2\text{O})_{29}]\}_{\infty}$: C, 30.0; H, 3.2; N, 13.7. Found: C, 29.8; H, 3.0; N, 13.9. IR (KBr pellet): ν (cm^{-1}) 3436 (s, br), 2098 (sh), 2046 (vs), 2016 (sh), 1630 (m), 1492 (m), 1428 (m), 1407 (m), 1384 (m), 1096 (w), 847 (w), 723 (w), 554 (w).

Data for **Os–Nd–BpymB.** Anal. Calcd for $\{[\text{Os}(\text{phen})(\text{CN})_4]_6\text{[Nd}(\text{H}_2\text{O})_{12}(\text{MeOH})(\text{bpym})_2(\text{H}_2\text{O})_{20}]\}_{\infty}$: C, 31.2; H, 3.0; N, 13.6. Found: C, 31.0; H, 2.5; N, 13.0. IR (KBr pellet): ν (cm^{-1}) 3434 (s, br), 2098 (sh), 2048 (vs), 2016 (sh), 1628 (m), 1493 (m), 1428 (m), 1406 (m), 1384 (m), 1095 (w), 847 (m), 723 (m), 554 (w).

Samples for photophysical analysis were prepared as above but using deuterated solvents (D_2O or CD_3OD) to minimize the presence of OH oscillators in the samples.

X-ray Crystallography. In all cases, a suitable crystal was mounted on a Bruker APEX-2 diffractometer equipped with graphite-monochromatized Mo K α radiation. Details of selected structural parameters are collected in Table 1, and details of the crystal, data collection, and refinement parameters are provided in Table 2. After integration of the raw data and merging of equivalent reflections, an empirical absorption correction was applied on the basis of a comparison of multiple symmetry-equivalent measurements.¹⁶ The structures were solved by direct methods and refined by full-matrix least-squares on weighted F^2 values for all reflections using the SHELX suite of programs.¹⁷ For coordinated and lattice water molecules, H atoms were added only when both of them showed up clearly in a refinement using only small-angle data; they were then fixed in position with O–H distances of 0.85 Å. In all cases, many of the lattice water molecules were refined with either 50 or 100% site occupancy as required to generate reasonable

thermal displacement parameters. In many cases, it was clear that the lattice solvent molecules were extensively disordered, and the assignments of the major electron density peaks as oxygen atoms represented an approximation. In particular, in the series **Os–Ln–PhenA**, the Na⁺ cation was disordered over two or three closely spaced sites. This caused problems in locating and refining the associated water ligands; numerous small electron density peaks, which we did not attempt to assign or refine, were apparent surrounding the region containing the disordered fractional Na⁺ ions. In all cases, however, the Os/Ln cyanide-bridged assemblies and any coordinated water molecules were clearly defined, with disorder being confined to the Na⁺ cations (where present) and/or lattice solvent molecules.

Acknowledgment. We thank the European Commission for a Marie Curie postdoctoral fellowship (Contract M1F1-CT-2005-513860) to S.G.B. and the EPSRC (U.K.) for Grant EP/E048390/1.

IC702353C

(16) Sheldrick, G. M. *SADABS: A Program for Absorption Correction with the Siemens SMART System*; University of Göttingen: Göttingen, Germany, 1996.

(17) *SHELXTL Program System*, version 5.1; Bruker Analytical X-ray Instruments Inc.: Madison, WI, 1998.